Level structure of ^{31}S via ^{32}S(p, d) ^{31}S

K. Setoodehnia,[1,*] A. A. Chen,[1] J. Chen,[1,†] J. A. Clark,[2] C. M. Deibel,[3,2,‡] J. Hendriks,[4] D. Kahl,[5,6] W. N. Lennard,[4] P. D. Parker,[7] D. Seiler,[8] and C. Wrede[9,10]

[1]*Department of Physics & Astronomy, McMaster University, Hamilton, Ontario, Canada L8S 4M1*
[2]*Physics Division, Argonne National Laboratory, Argonne, Illinois 60439, USA*
[3]*Joint Institute for Nuclear Astrophysics, Michigan State University, East Lansing, Michigan 48824, USA*
[4]*Department of Physics & Astronomy, Western University, London, Ontario, Canada N6A 5B7*
[5]*Center for Nuclear Study (CNS), the University of Tokyo, Wako Branch at RIKEN, Wako, Saitama 351-0198, Japan*
[6]*School of Physics and Astronomy, University of Edinburgh, Edinburgh EH9 3FD, Scotland*
[7]*Wright Nuclear Structure Laboratory, Yale University, New Haven, Connecticut 06520, USA*
[8]*Physik Department, Technische Universität München, D-85748 Garching, Germany*
[9]*Department of Physics, University of Washington, Seattle, Washington 98195, USA*
[10]*Department of Physics & Astronomy and National Superconducting Cyclotron Laboratory, Michigan State University, East Lansing, Michigan 48824, USA*

(Received 21 June 2020; revised 9 August 2020; accepted 28 September 2020; published 14 October 2020)

Background: Properties of proton-unbound ^{31}S states determine the ^{30}P(p, γ) ^{31}S reaction rate, which has a significant impact on explosive hydrogen burning in classical novae and type-I x-ray bursts. Despite several previous studies, uncertainties still remain with respect to the nuclear structure of ^{31}S near the proton threshold.
Purpose: The level structure of ^{31}S has been presently investigated via a charged-particle spectroscopy experiment using the ^{32}S(p, d) ^{31}S reaction.
Method: Deuterons corresponding to ^{31}S excited states with $3.285 \leqslant E_x \leqslant 10.8$ MeV were momentum analyzed via an Enge split-pole spectrograph at six laboratory angles between 10° and 62°. Differential cross sections of the ^{32}S(p, d) ^{31}S reaction were measured at $E_p = 34.5$ MeV. Distorted-wave Born approximation calculations were performed to constrain the spin-parity assignments of several of the observed levels.
Results: We have detected 72 excited states of ^{31}S, out of which 17 are within the astrophysical region of interest corresponding to the temperature range of 0.1–1.5 GK. We have resolved the discrepancy in the spin and parity of an excited state with $E_x = 6542$ keV, showing that is it not $J^\pi = 3/2^-$, and therefore the contribution of this state to the ^{30}P(p, γ) reaction rate is likely much less significant than previously thought owing to the larger angular-momentum transfer required to populate this excited state. Moreover, our measurement results help consolidate the spin-parity assignments for the 6377 and 6636 keV states in ^{31}S.
Conclusions: This work presents the most comprehensive spin-parity assignments to date from a single-neutron transfer reaction on ^{32}S to ^{31}S excited states in the region between 6 to 7 MeV excitation energy. This region is significant for the determination of the ^{30}P(p, γ) ^{30}S reaction rate over the temperatures characteristic of explosive hydrogen burning in novae.

DOI: 10.1103/PhysRevC.102.045806

I. INTRODUCTION

Explosive hydrogen burning in classical novae occurs in close binary star systems, where extreme temperatures and densities are achieved on the compact accreting stars. In such binary systems consisting of a white dwarf as the compact star, hydrogen-rich matter is accreted onto the surface of the white dwarf from a main sequence companion star overflowing its Roche lobe. Gravitational compression heats the bottom layers of the accreted envelope. When the temperature of these layers increases to ≈20 MK [1], the hydrogen starts fusing into helium. The generation of a large amount of energy as a result of nuclear reactions finally triggers explosive hydrogen burning via a thermonuclear runaway in the accreted envelope, which leads to a classical nova outburst. Simulations [2] of oxygen-neon (ONe) novae show that peak temperatures reached in the thermonuclear runaway are typically in the 0.1–0.4 GK range, and the nova ejecta shows significant nuclear processing. Classical nova outbursts are thought to be the major source of ^{15}N, ^{17}O and to some extent ^{13}C in the galaxy [3] and contribute to the abundances of other species with

*Present Addresses: European X-ray Free Electron Laser GmbH, Holzkoppel 4, 22869 Schenefeld, Germany; kiana.setoodehnia@xfel.eu
†Present Address: National Superconducting Cyclotron Laboratory, East Lansing, Michigan 48824, USA.
‡Present Address: Department of Physics & Astronomy, Louisiana State University, Baton Rouge, Louisiana 70803, USA.

masses up to $A \approx 40$, including ^{26}Al, which is synthesized in ONe novae.

The nucleosynthesis of ONe novae has been simulated via postprocessing [2,4] and hydrodynamic [5,6] nucleosynthesis models. These studies have consistently found the $^{30}\mathrm{P}(p,\gamma)^{31}\mathrm{S}$ reaction rate to be the driver for nuclear activity in ONe novae in the mass region above $A = 30$. Therefore, the $^{30}\mathrm{P}(p,\gamma)$ reaction is known to be one of a few whose rate uncertainty over the temperature range of interest for novae significantly affects the abundances of a large number of observable isotopes [7].

The effects of the uncertain thermonuclear rate of the $^{30}\mathrm{P}(p,\gamma)^{31}\mathrm{S}$ reaction on our understanding of classical novae, and their nucleosynthesis modeling have been extensively reviewed in Ref. [8]. In particular, a previous uncertainty of four orders of magnitude in the $^{30}\mathrm{P}(p,\gamma)^{31}\mathrm{S}$ rate [2] resulted in a factor of ≈800 spread in the predicted abundance of ^{30}Si (see Table 7 in Ref. [2]). The $^{30}\mathrm{Si}/^{28}\mathrm{Si}$ abundance ratio serves as an important marker for identifying novae as candidate sources for presolar meteoritic grains [9]. Furthermore, the $^{30}\mathrm{P}(p,\gamma)^{31}\mathrm{S}$ rate uncertainty affects some of the nova thermometers, e.g., the O/S, S/Al, O/P, and P/Al abundance ratios, by factors of ≈3–6 [10].

In addition, variations in the $^{30}\mathrm{P}(p,\gamma)^{31}\mathrm{S}$ reaction rate have a large impact on the Si/H abundance ratio. The latter is, in turn, used as a nova mixing meter [11] to infer the degree of mixing that occurs between the outer layers of the underlying white dwarf and the accreted envelope prior to the thermonuclear runaway. It is shown [11] that the mixing meters are generally robust with regard to variations in thermonuclear reaction rates. However, the Si/H abundance ratio is an exception due to the uncertainty in the $^{30}\mathrm{P}(p,\gamma)^{31}\mathrm{S}$ reaction rate.

Beyond the aforementioned effects in novae, the $^{30}\mathrm{P}(p,\gamma)^{31}\mathrm{S}$ reaction also becomes important for simulations of nucleosynthesis in type-I x-ray bursts, which, in addition to classical novae, are among the astrophysical sites where explosive hydrogen burning takes place.

Type-I x-ray bursts result from thermonuclear runaways in hydrogen- and helium-rich material accreted onto the neutron-star surface in an x-ray binary system [12,13]. The nuclear fuel is consumed through the αp and rp processes [14–16]. The $^{30}\mathrm{P}(p,\gamma)^{31}\mathrm{S}$ reaction rate is a significant input for rp-process calculations [17] and has been shown to be one of the main reactions governing the flow as the burst temperature approaches its peak ($T \approx 1.5$ GK) [18].

Over the temperature ranges characteristic of explosive hydrogen burning in novae and type-I x-ray bursts, the properties, e.g., resonance energies, partial widths, and spin-parity assignments, of $^{30}\mathrm{P}+p$ resonances corresponding to ^{31}S excited states in the energy range of about $6 \lesssim E_x \lesssim 7.5$ MeV are crucial for evaluating the rate of the $^{30}\mathrm{P}(p,\gamma)^{31}\mathrm{S}$ reaction [$Q = 6130.9(4)$ keV [19]].

^{30}P is radioactive (terrestrial $t_{1/2} = 2.498(4)$ m [20]), and a beam with sufficient intensity ($>10^6$ pps [7,21]) at the energies of astrophysical interest is currently unavailable. Therefore, the level properties of ^{31}S have to be investigated with indirect methods. Extensive experimental work has already been performed [7,22–35] to investigate the level properties of the astrophysically important resonances. Reference [8] has reviewed all the relevant experimental and theoretical work which has been performed up to 2014. Despite these measurements and simulations, the $^{30}\mathrm{P}(p,\gamma)^{31}\mathrm{S}$ reaction rate remains uncertain due to the incompleteness of and inconsistencies in the data available in the literature.

To address inconsistencies and improve our current understanding of the levels of ^{31}S above the proton threshold, we have measured the $^{32}\mathrm{S}(p,d)^{31}\mathrm{S}$ reaction. It was part of a dataset acquired when measuring $^{32}\mathrm{S}(p,t)$ [36–38].

The results of our $^{32}\mathrm{S}(p,d)$ measurement could help facilitate the analysis of two recent measurements performed at the Texas A&M Cyclotron Institute [39] and at TRIUMF [40]. The former experiment measured the $^{32}\mathrm{S}(p,d)^{31}\mathrm{S}$ reaction (at essentially the same energy as that of our measurement) to study the γ rays and proton decays of the deexciting ^{31}S states. The experiment at TRIUMF measured the $^{3}\mathrm{He}(^{32}\mathrm{S},\alpha\gamma)^{31}\mathrm{S}$ reaction in inverse kinematics to study lifetimes of ^{31}S states. Both of these measurements suffered from relatively poor excitation energy resolution. Consequently, one of the challenges of the data analysis is understanding which states are observed in single-neutron-removal reactions from ^{32}S. The present work will shed light on this issue.

II. EXPERIMENTAL SETUP AND DATA ANALYSIS

The experiment was performed between 2008 and 2010 at the Wright Nuclear Structure Laboratory (WNSL) at Yale University. Protons were accelerated by the extended stretched transuranium (ESTU) tandem Van de Graaff accelerator to 34.5 MeV ($\Delta E/E \approx 6 \times 10^{-4}$) with intensities of up to 90 enA, and focused to a spot size of 2 mm diameter on target.

Two types of targets were employed: 249 ± 25 μg/cm^2 of CdS evaporated onto a 20-μg/cm^2-thick natural carbon foil, and a 55.9 ± 5.6 μg/cm^2 isotopically pure (99.9% enriched) ^{12}C foil implanted with 10.4 ± 0.4 μg/cm^2 of ^{32}S.

The thickness of the CdS target was determined prior to our experiment by measuring, using a silicon surface barrier detector, the energy loss of α particles from the decay of a ^{241}Am source passing through this target. The uncertainty in the target thickness was estimated to be 10% from a conservative estimate of the uncertainty of stopping powers of helium in CdS from SRIM [41], where no experimental data are available. The thickness of the sulfur content of the CdS target was determined to be 53 ± 5 μg/cm^2 through measurement of elastic scattering of an 8 MeV ^{4}He beam off of the CdS target. This experiment was performed separately prior to our (p,d) measurement. The aforementioned thickness of the sulfur content was later used in the determination of the differential cross sections of the ^{31}S excited states discussed in this work. The implanted target was fabricated [42] specifically to reduce the relatively flat background produced by the $^{\mathrm{nat}}$Cd (where nat refers to natural isotopic abundance) component of the CdS target. The thickness and chemical composition of the implanted target were determined via a Rutherford backscattering spectrometry measurement performed prior to this work (see Refs. [37,42]). In addition to the aforementioned targets, we used a natural silicon target

for calibration purposes, and a ^{nat}Cd foil supported by a natural carbon substrate, together with isotopically enriched ^{12}C and ^{13}C foils for background-subtraction purposes. These targets and the method of measuring their thicknesses are described in Ref. [37]. Finally, no evidence for peak broadening and/or a change of peak shape was observed during the experiment, indicating that there was no target degradation over time. Moreover, there is published evidence [43] that sulfur-implanted carbon foils do not degrade under beam bombardment.

Deuterons were dispersed according to their momentum-to-charge ratio with a high-resolution Enge split-pole magnetic spectrograph, the technical specifications of which are given in Refs. [36,38]. The horizontal and vertical solid angle acceptances of the spectrograph at each laboratory angle were determined by using two sets of micrometers as slits, whose positions were carefully calibrated prior to our experiment.

The beam current was integrated by using a beam current integrator module together with a beam stop, located inside the target chamber, which was biased at +600 V in order to reabsorb the electrons boiling off the beam stop after stopping the beam.

The study was carried out at multiple laboratory angles of 10°, 20°, 22°, and 62° using the CdS target, and at 22°, 27.5°, and 45° using the implanted target.

The detection system is described in detail elsewhere [36–38]. Identification of deuterons was carried out by measuring their energy loss, residual energies, and positions along the focal plane of the spectrograph. The spectra of the deuterons' momenta were then plotted for each spectrograph angle (see Figs. 1 and 2). Deuteron peaks corresponding to ^{31}S excited states in these spectra were clearly identified through kinematic analysis.

The major contaminant peaks present in the spectra were the ground state, the 2, 4.3, 4.8, 6.3, and 6.5 MeV excited states [44] of ^{11}C, populated via the ^{12}C$(p,d)^{11}$C reaction, and the 6.18 MeV excited state [45] of ^{15}O, populated via the ^{16}O$(p,d)^{15}$O reaction (see Figs. 1 and 2). According to the simulations of positions of excited states along the focal plane, a few more low-lying states of ^{15}O could be on the focal plane; however, we did not find any statistical evidence of these states in our spectra. The ground state and the 6.3 and 6.5 MeV excited states of ^{11}C were only observed at 62° and 27.5°, respectively, since the population of different states on the focal plane depends on their cross section as a function of the scattering angle at which the reaction is measured. Also, the states were shifted on the detection plane when the spectrograph's angle was changed, and thus the aforementioned states were kinematically excluded at other angles.

Apart from a few deuteron peaks observed in the presented spectra, which were fit by using Gaussian-plus-exponential functions to account for their exponential tails, the rest of the spectral analysis for deuteron peaks was similar to the procedure used for triton peaks from the ^{32}S$(p,t)^{30}$S reaction, which is described in Refs. [36–38]. For the purposes of fitting, we have assumed the states to be narrow compared with the instrumental resolution. The energy calibration was determined from a combination of known levels of ^{27}Si [measured with the ^{28}Si(p,d) reaction using the Si-target], ^{11}C (produced by the carbon substrate in both targets), and ^{31}S. The adopted energies of ^{27}Si levels were weighted averages of the previous work [46–48], and those of ^{11}C were taken from Ref. [44]. For ^{31}S internal calibration points, we used the weighted average energies between the more recent results of Refs. [7,23,24,26,27,29,33,35] for states with 3285 keV $\leqslant E_x \leqslant$ 7051 keV; and the adopted energies of Ref. [49] for the states with $E_x >$ 7051 keV. To derive the weighted average energies, a 3 keV systematic uncertainty in the results of Ref. [7] was also taken into account.

At each angle, polynomial least-squares fits of second or third degree ($0.9 \leqslant \chi^2_\nu \leqslant 1.4$; $0.56 \leqslant p \leqslant 0.71$) of momentum vs centroid channel were determined for these calibration points. These fits were used to determine the ^{31}S excitation energies at each angle. The final excitation energy uncertainties for the data at each angle arise from (1) statistical uncertainties (on average $\leqslant$3 keV), (2) uncertainties in the thicknesses of the implanted target (2 keV) and the CdS target (3 keV) taking into account the uncertainty in the thickness of the ^{nat}Si target used for calibration, (3) uncertainty in the Q values of the ^{28}Si(p,d) and ^{32}S(p,d) reactions (0.14 keV [50] and 0.24 keV [50,51], respectively), and (4) 20 keV uncertainty in the beam energy ($\leqslant$0.4 keV uncertainty in excitation energy). Therefore, apart from the statistical uncertainties, at each angle the systematic uncertainties in ^{31}S excitation energies, when added in quadrature, were 3 and 2.1 keV for the CdS and implanted targets, respectively. Lastly, to obtain the final ^{31}S excitation energies, a weighted average was calculated for each state over all the angles, and thus over both targets. In a few cases where the uncertainty in the weighted average was smaller than the smallest uncertainty in the measured excitation energies, the latter was adopted as the final uncertainty only if the energy was measured at fewer than four laboratory angles.

The energy resolution at full width at half maximum (FWHM) was ≈38 keV and ≈30 keV for the spectra obtained with the CdS and implanted targets, respectively. Therefore, our achieved energy resolution is a factor of two to four better than those of the previous ^{32}S$(p,d)^{30}$S measurement [24]. It should be noted that, as the scattering angle increases, the energy resolution gets worse because of kinematic broadening due to an increase in the energy straggling of the deuterons through the target. The present energy resolutions are averages over all angles measured with a given target.

III. RESULTS

In the present work, a total of 72 excited states of ^{31}S with $3.285 \leqslant E_x \leqslant 10.8$ MeV were observed (see Tables I and II), of which (i) 17 are within the astrophysical region of interest corresponding to the temperature range of 0.1–1.5 GK, and (ii) 10 are tentatively new states all of which are above 9 MeV in excitation energy and are thus not of interest to explosive hydrogen burning at the aforementioned temperature range.

Most of the measured energies in the present work are in agreement within 1σ–2σ with those measured in the previous ^{32}S$(p,d)^{31}$S measurement [24], as well as with the adopted energies of Refs. [7,26–29,33,35,49].

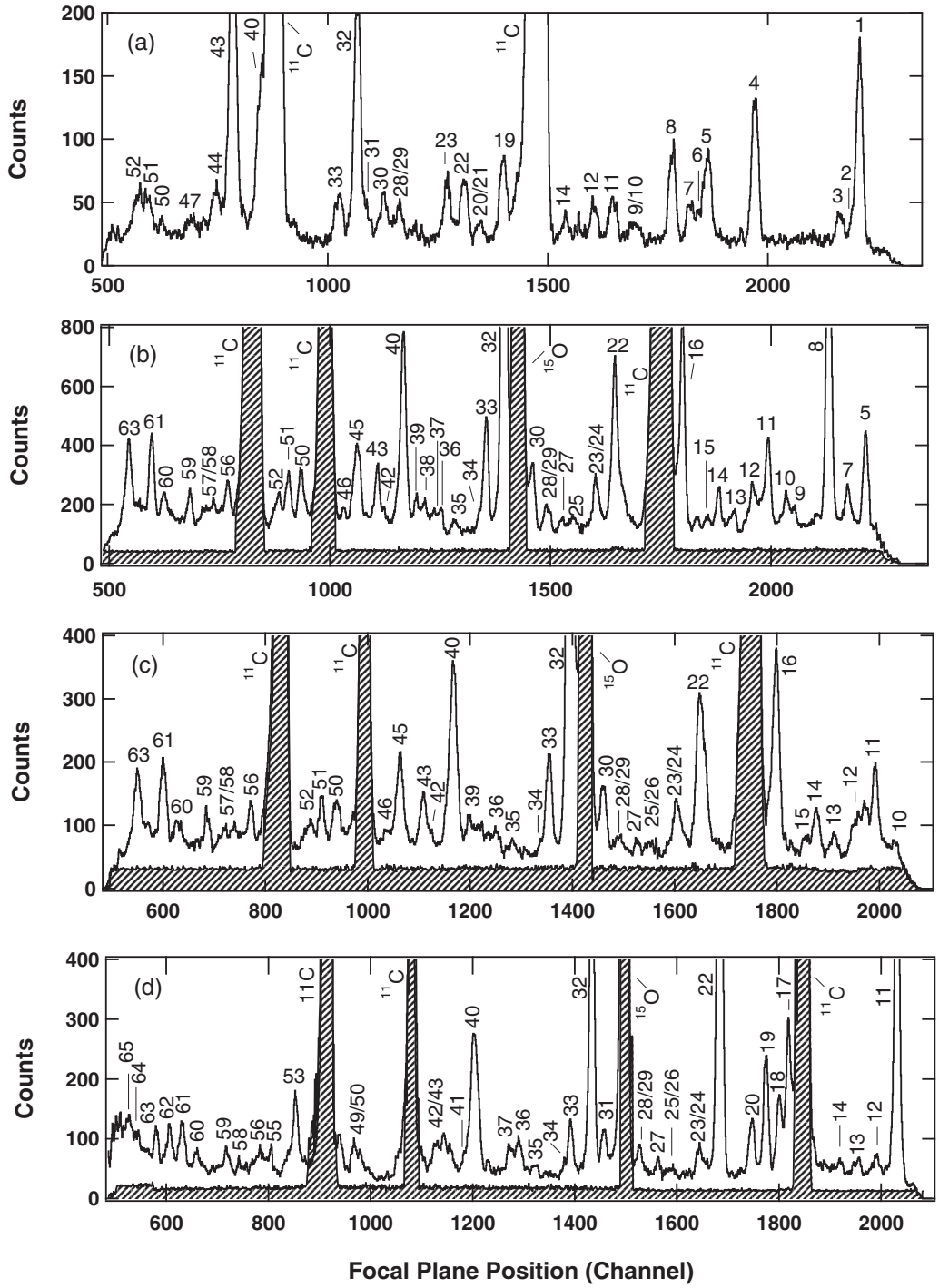

FIG. 1. Deuteron spectra measured from the ^{32}S$(p,d)^{31}$S reaction at (a) 62°, (b) 22°, (c) 20°, and (d) 10° obtained with the CdS target. ^{31}S states are labeled with peak numbers corresponding to energies shown in Tables I and II. Contaminant peaks are labeled by their parent nuclei. The shaded histograms are background spectra measured with a $^{\text{nat}}$Cd foil supported by a natural carbon backing, scaled to the background peaks of the ^{32}S$(p,d)^{31}$S data. The background was not measured at 62°. For 10° and 20°, an aluminum plate along the focal plane blocked the region corresponding to channels $\geqslant$2100, where elastically scattered protons reached the focal plane.

The relative differential cross sections in the laboratory system were obtained from the procedure presented in Ref. [37] (see Chapter 3) and Ref. [38]. The measured differential cross sections in the laboratory system were converted to those in the center-of-mass system following the formalism presented in Appendix C of Ref. [52]. The uncertainties in the experimental differential cross sections are dominated by the statistical uncertainties in the areas under each peak. The systematic uncertainties in the differential cross sections are dominated by the target thickness uncertainties, which amount to 9% for the sulfur content of the CdS target and 4% for the implanted target. The uncertainties in other factors

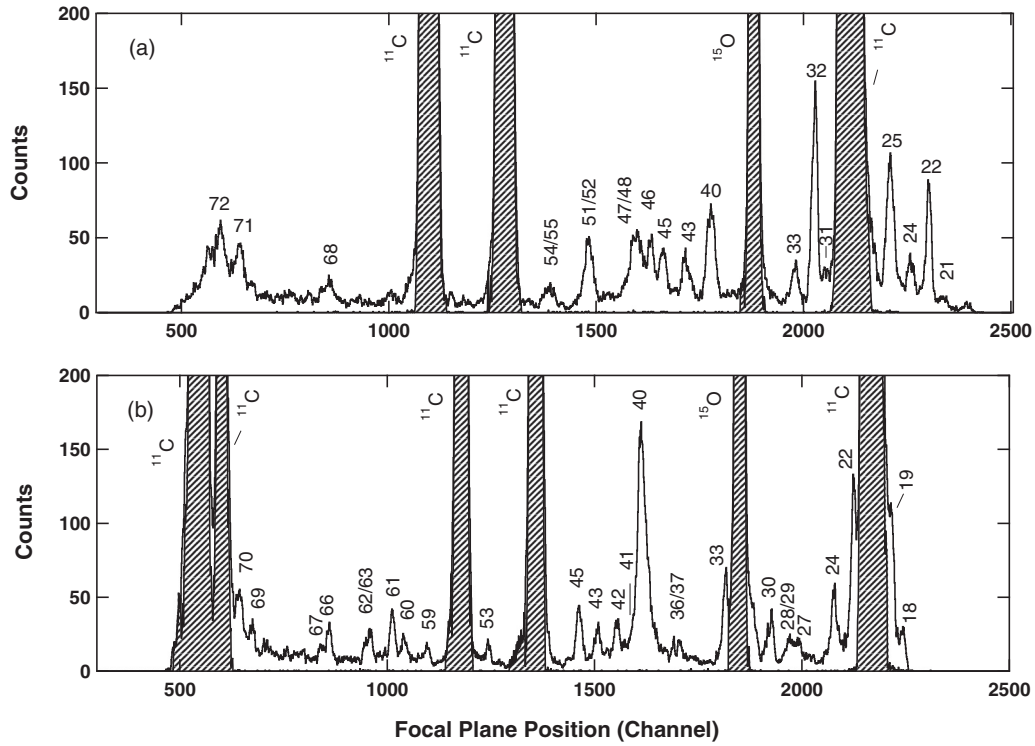

FIG. 2. Deuteron spectra from the ^{32}S(p, d) ^{31}S reaction measured at (a) 45° and (b) 27.5° obtained with the implanted target. ^{31}S states are labeled with peak numbers corresponding to energies shown in Tables I and II. Contaminant peaks are labeled by their parent nuclei. The shaded histograms are background spectra measured with an isotopically enriched ^{12}C target, scaled to the background peaks of the ^{32}S(p, d) ^{31}S data. For 27.5°, an aluminum plate along the focal plane blocked the region corresponding to channels between ≈2300–2500, where elastically scattered protons reached the focal plane. The 22° spectrum obtained with the implanted target is not shown due to low statistics.

such as solid angle and total accumulated charge are negligible.

The only angle at which the experimental differential cross sections were measured using both targets was 22°. The spectrum obtained at this angle with the implanted target suffers from low statistics. Therefore, we only calculated differential cross sections for the well-populated calibration peaks. The results are consistent with those measured at the same angle using the CdS target.

To obtain the spin-parity assignments of ^{31}S states observed in the present work, the theoretical angular distributions of the cross sections were computed via distorted-wave Born approximation (DWBA) calculations using the one-step finite-range transfer formalism via DWUCK5 [53]. These calculations were carried out only for those ^{31}S states of astrophysical interest observed in the present work over at least four laboratory angles.

The distorted waves in the entrance and exit channels were calculated for optical interaction potentials, the parameters of which were taken from Ref. [54] (and references therein), and are given in Table III. Furthermore, to describe the interaction of ^{31}S $+n \rightarrow$ ^{32}S, a volume Woods-Saxon potential with the addition of the Thomas spin-orbit factor was used (see Table III). Reference [24] seems to have used this same potential for the $p + n \rightarrow d$ interaction. We, on the other hand, have used the widely used Reid soft core potential [55] to derive the deuteron wave function, as well as the p-n interaction. In addition, in our DWUCK5 input files, according to the instructions presented in Ref. [53], we have reduced the strength of the imaginary potential for surface absorption (W_D) by $4a_I$, where a_I is the imaginary diffuseness parameter. This *may not* be the case in Ref. [24], which could be one of the factors (apart from different beam energies) that explains the difference in the present $J^\pi = 1/2^+$ theoretical DWBA curves vs those of Ref. [24].

Deuteron angular distribution plots are shown in Fig. 3. The theoretical deuteron angular distribution curves were scaled to the experimentally determined center-of-mass differential cross sections using linear fits with zero intercepts.

For $\ell > 0$ transfers, since the angular distributions depend very weakly on the total angular momentum, we could not differentiate between $\ell \oplus s$ transitions, where s is the spin of the transferred neutron.

In the following, we discuss our spin and parity assignments for some of the states observed in the present work and briefly review some of the observed states.

IV. DISCUSSION

The 5156.3 keV level. This level is known to be a $1/2^+$ state [26,29,35], and our deuteron angular distribution data are consistent with $J^\pi = 1/2^+$ [see Fig. 3(a)].

The 5301 keV level. This state is another ^{31}S state whose spin-parity was established previously to be $9/2^+$ [26,29].

TABLE I. Weighted average (over all angles) excitation energies (in keV) of ^{31}S from the present work in comparison with those measured in selected previous works. States used in the present work for energy calibration are marked with an asterisk. The astrophysical region of interest for explosive hydrogen burning in novae and type-I x-ray bursts ($0.1 \leqslant T \leqslant 1.5$ GK) corresponds to 6 MeV $\lesssim E_x(^{31}\mathrm{S}) \lesssim$ 7.5 MeV. The states in square brackets are states with tentative detection. Peak numbers are displayed in Figs. 1 and 2.

(p,d) [24]		$(^3\mathrm{He},t)$ [7]		$(\alpha,n\gamma)$ [27,29]		2013 Evaluation [49]		(d,t) [28]	$(\beta\gamma)$ [33,35]		(p,d) Present Work		Peak	
E_x (keV)	J^π	E_x (keV)[a]	J^π	E_x (keV)	J^π	E_x (keV)	J^π	E_x (keV)[b]	E_x (keV)	J^π	E_x (keV)	J^π	Adopted J^π	Number
				3284.7(2)	$5/2^+$	3284.67(16)	$(5/2)^+$		3283.76(31)	$5/2^+$	3284.7*			1
				3351.3(2)	$7/2^+$	3351.30(19)	$(7/2)^+$		3349.30(32)	$7/2^+$	3353(5)			2
				3433.3(5)	$3/2^+$	3435.7(3)	$3/2^+$		3434.90(33)	$3/2^+$	3438(3)			3
4085(2)	$5/2^+$			4086.1(16)	$5/2^+$	4080.0(100)	$3/2^+, 5/2^+$		4085.4(8)	$5/2^+$	4083(3)			4
				4208.3(5)	$3/2^+$	4209.15(18)	$(1/2,3/2,5/2)^+$		4207.7(31)	$3/2^+$				
4446(6)	$7/2^-$			4449.6(3)	$7/2^-$	4450.65(25)	$(7/2)^-$				4450(3)			5
				4527.8(2)	$3/2^+$	4520.5(3)	$3/2^+$		4519.63(32)	$3/2^+$	4518(6)			6
				4583.4(3)	$7/2^+$	4583.98(24)	$(7/2)^+$				4580(3)			7
4707(3)	$5/2^+$			4710.1(8)	$5/2^+$	4707.0(30)	$3/2^+, 5/2^+$		4717.72(32)	$5/2^+$	4712(2)			8
				4867.5(3)	$1/2^+$	[4867.5 4]	$(1/2^-, 3/2^-)$		4866.2(6)	$1/2^+$				
4988(8)	$3/2^-$			4971.2(20)	$(1/2^-, 3/2^-)$	4971.0(30)	$(3/2)^-$		4970.7(9)	$3/2^-$	4975(4)			9
				5023.9(3)	$5/2^+$	5022.0(30)			5021.9(5)	$5/2^+$	5023(3)			10
5155(5)	$1/2^+$			5157.5(20)	$1/2^+$	5157.5(3)	$1/2^+$		5156.1(6)	$1/2^+$	5156.3*	$1/2^+$	$1/2^+$	11
5331(5)	$9/2^+$			5301.7(3)	$9/2^+$	5300.7(3)	$(9/2^+)$				5301(2)	$7/2^+, 9/2^+$	$9/2^+$	12
				5401.5(8)	$5/2^+$	5408.2(9)					5402(2)	$5/2^{(-)}$	$5/2^{(-)}$	13
						5439.0(30)			5435.9(9)	$3/2^+$				
5497(10)	$5/2^+$			5518.3(3)	$5/2^+$	5518.0(30)	$3/2^+, 5/2^+$				5517(2)	$3/2^+, 5/2^+$	$5/2^+$	14
				5675.8(6)	$7/2^+$	5678.0(30)					5678(3)			15
5781(5)	$5/2^+$					5775.0(30)	$3/2^+, 5/2^+$		5775.4(4)	$5/2^+$	5775(2)			16
						5824.0(30)					5829(4)			17
5959(10)[c]	$(3/2^+, 5/2^+)$			5891.5(20)	$3/2^+$	5896.0(30)	$3/2^+, 5/2^+$		5890.3(8)	$3/2^+$	5893(3)			18
5959(10)[c]	$(9/2^+)$			5977.2(7)	$(9/2^+)$	5977.9(7)	$(9/2^+)$				5979(3)			19
		6136(3)	9/2	6138.3(21)	$(3/2,7/2)^+$	6138.6(6)	$(7/2^+)$		6129.3(10)	$5/2^+$	6139(4)			20
		6160(3)	5/2	6158.5(5)	$7/2^+$	6160.0(6)	$(5/2^-, 7/2^+)$				[6159(3)]			21
6267(5)	$1/2^+$	6260(3)	$1/2^+$			6255.3(5)	$1/2^+$		6255.0(6)	$1/2^+$	6255.6*	$1/2^+$	$1/2^+$	22
		6284(3)	$3/2^+$			6280.60(16)	$3/2^+$		6279.0(6)	$3/2^+$				
		6329(3)	$1/2^+$	6327.0(5)	$3/2^-$	6327.0(5)	(3/2)							
		6356(3)	$3/2^+$	6357.3(2)	$5/2^-$	6357.32(22)	$(5/2^-)$	6356(2)						
		6378(3)	9/2	6376.9(4)	$9/2^-$	6376.7(3)	$(9/2^-)$				6377(3)	$9/2^-, 11/2^-$	$9/2^-$	23
				6392.5(2)	$5/2^+$	6392.43(22)	$(5/2^+)$		6390.2(7)	$3/2^+$	6390.8(17)	$3/2^+, 5/2^+$	$3/2^+, 5/2^+$	24
		6395(4)		6394.2(2)	$11/2^+$	6394.36(22)	$(11/2^+)$	6394(1)						

TABLE I. (*Continued.*)

(p, d) [24]		$(^3\mathrm{He}, t)$ [7]		$(\alpha, n\gamma)$ [27,29]		2013 Evaluation [49]		(d, t) [28]	$(\beta\gamma)$ [33,35]		(p, d) Present Work			Peak
E_x (keV)	J^π	E_x (keV)[a]	J^π	E_x (keV)	J^π	E_x (keV)	J^π	E_x (keV)[b]	E_x (keV)	J^π	E_x (keV)	J^π	Adopted J^π	Number
6411(9)	$11/2^+$	6403(4)				6401.1(30)		6402(2)						
6546(15)	$5/2^-$	6543(3)	(7/2,9/2)	6541.9(4)	$3/2^-$	6541.9(4)	$(3/2^-)$	6543(2)			6542(3)	$(7/2^+, 9/2^-, 11/2^+)$	$7/2^+$	25
		6586(3)	7/2	6583.1(20)	$(5/2,7/2)^-$	6582.9(20)	(7/2)	6584(1)			6585(3)			26
		6637(3)	9/2	6636.1(7)	$9/2^-$	6636.3(3)	$(9/2^-)$				6636(2)	$7/2^+, 9/2^\pm, 11/2^+$	$9/2^-$	27
		6720(3)	5/2			6720.0(20)	(5/2)	6720(1)						28/29[d]
		6749(3)	$3/2^+$			6749.0(20)	$3/2^+$	6748(3)						28/29[d]
6848(9)[c]	$11/2^-$	6835(3)	11/2			6833.2(3)	$(11/2^-)$				6833.9(12)	$7/2^+, 9/2^-, 11/2^-$	$9/2^-, 11/2^-$	30
6848(9)[c]	$(3/2^-, 5/2^+)$	6870(3)	11/2			6872.0(20)	(11/2)	6869(2)						
		6936(4)				6937.0(20)	$(1/2^+, 3/2^+, 5/2^+)$	6935(2)						
		6958(4)				6961.0(30)		6958(2)			6960(4)			31
		6971(4)				6975.0(30)	$1/2^+$	6971(2)						
7044(6)	$5/2^+$	7030(4)				7037.0(20)	$3/2^+, 5/2^+$				7035.4*	$3/2^+, 5/2^+$	$3/2^+, 5/2^+$	32
		7049(4)				7052.0(20)			7050.0(8)	$1/2^+$				
7144(16)	$(3/2,5/2)^+$					7156.0(20)	$3/2^+, 5/2^+$		7149.8(9)	$5/2^+$	7157.7(11)	$3/2^+, 5/2^+$	$5/2^+$	33
						7196.0(20)					[7197(2)]			34
						7304.0(5)	$(11/2^+)$				7306(9)			35
						[7376.0(30)]								
						7469.0(30)					7469(3)			36
						7501.0(30)								
7510(6)						7517.0(30)	$1/2^+, 3/2^+, 5/2^+$				7518(2)			37

[a]The ±3 keV systematic uncertainty for the energies of Ref. [7] has been taken into account for the energies listed in this column.
[b]The excited states used for energy calibration in this measurement are not listed in this column.
[c]Unresolved doublet [24].
[d]We observe evidence for this state but it is unresolved. For more explanation, see Sec. IV.

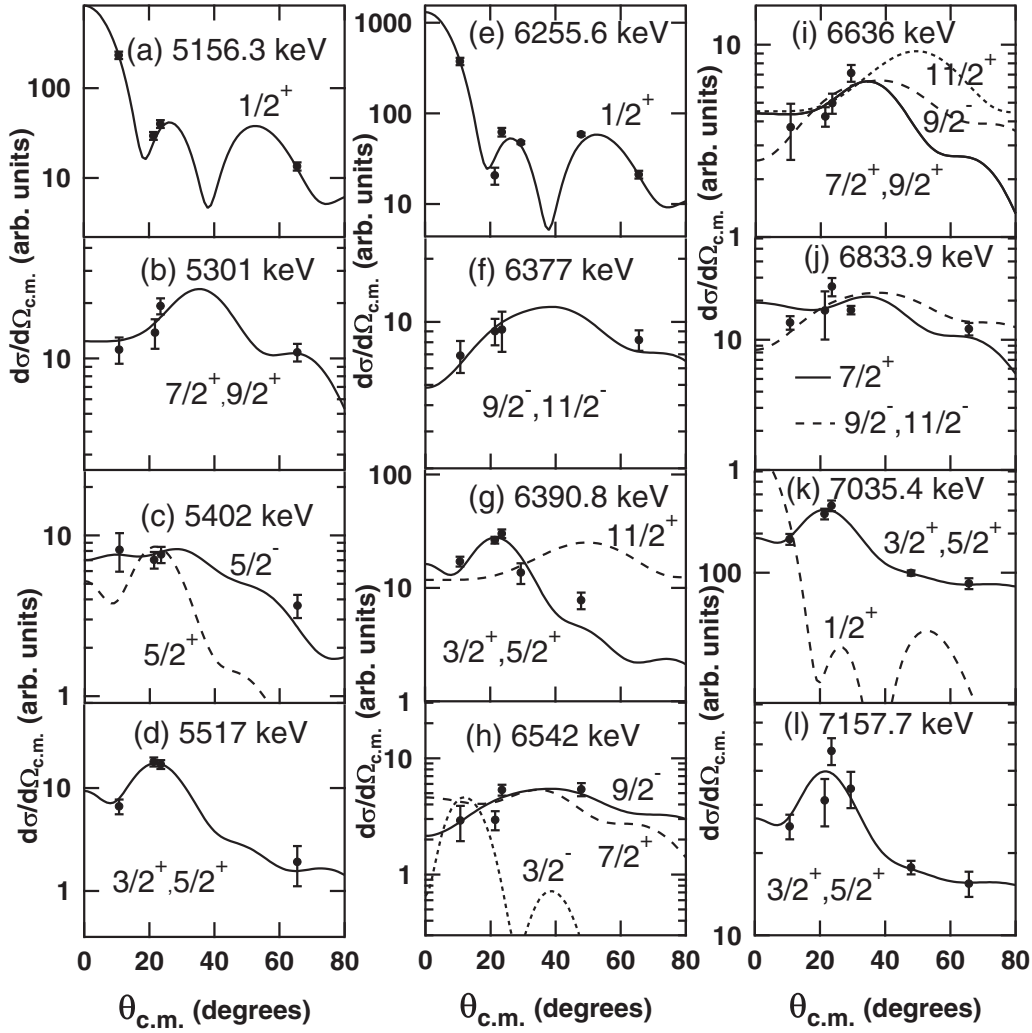

FIG. 3. Deuteron angular distributions populating states of ^{31}S compared with the theoretical DWBA curves. The filled circles with error bars (statistical in nature) are the measured relative differential cross sections in the center-of-mass system given in arbitrary units; and the solid, dashed, and dotted curves are the theoretical angular distributions obtained using DWUCK5 [53]. If not shown, the error bar is smaller than the point size. The excitation energies (in keV) are given on the top middle of each plot.

Our deuteron angular distribution data are consistent with this assignment but the $J^\pi = 7/2^+$ assignment is also equally compatible with our data [see Fig. 3(b)]. Since $J^\pi = 9/2^+$ assignment is already established, we disfavor $J^\pi = 7/2^+$ and adopt $J^\pi = 9/2^+$.

The 5402 keV level. The spin of this state was tentatively determined [26], based on mirror assignments, to be between a wide range of $3/2$ to $7/2$ with an unknown parity. Recently, Doherty *et al.* [29] assigned this level to be a $5/2^+$ state. The present forward-angle deuteron angular distribution data are reasonably consistent with this spin assignment but are best fit with a negative parity instead [see Fig. 3(c)].

The 5517 keV level. Similar to the 5402 keV state, the spin of this state was determined [26], based on mirror assignments, to be within $J^\pi = 3/2$–$7/2$ with an unknown parity. In the recent work of Ref. [29], its J^π value is firmly given as $5/2^+$, which agrees well with our present deuteron angular distribution data [see Fig. 3(d)].

The 6139 and 6159 keV levels. The energy difference between these levels is less than our experimental energy resolution. We observe a somewhat wider than usual peak at 60° (labeled as peak 20/21 in Fig. 1). When fit with a doublet, the energies are consistent with these levels. At 45°, we observe a small peak whose width is consistent with that of a single peak in that spectrum and when calibrated, the energy is consistent with the 6159 keV state. The 6139 and 6159 keV states seem to have disappeared at 22° and 20° and are obscured by the carbon contamination of the target at 27.5°. At 10°, we only observe the 6139 keV state.

The 6255.6 keV level. We observe a prominent peak at every angle, which we identify with this state. It is known [7,24,26,34,35,56] to have $J^\pi = 1/2^+$. The present deuteron angular distribution data are best fit by an $\ell = 0$ angular-momentum transfer, which leads to an unambiguous assignment (since the J^π value of the ^{32}S target is 0^+) of $J^\pi = 1/2^+$ to this state [see Fig. 3(e)].

TABLE II. High-energy excited states of ^{31}S measured in the present work in comparison with those of the latest evaluation of Ref. [49]. To make the table brief, those states not observed in the present work are omitted. The states in square brackets are ones with tentative detection, and those used in the present work for energy calibration are marked with an asterisk. Being outside the energy range of interest, we did not perform distorted-wave Born approximation calculations for these states.

2013 Evaluation [49]		Present work	
E_x (keV)	J^π	E_x (keV)	Peak number
7585(3)		7584(2)	38
7644.5(8)	$(1/2^+, 3/2^+, 5/2^+)$	7640(2)	39
7724(3)	$(1/2^-, 3/2, 5/2)$	7724*	40
7744(3)		[7743(2)]	41
7894(3)	$(1/2^+, 3/2^+, 5/2^+)$	7895(2)	42
7907(3)	$1/2^+$	7907*	43
8022(3)	$(1/2^+, 3/2^+, 5/2^+)$	[8024(2)]	44
8045(3)	$1/2^+, 3/2^+, 5/2^+$	8044.5(12)	45
8131(3)		8130(2)	46
[8209(3)]		[8211(2)]	47
8229(3)		[8221(4)]	48
8382(10)		8386(3)	49
8426(4)	$(1/2^+, 3/2^+, 5/2^+)$	8422(2)	50
8498(3)	$1/2^+$	8498*	51
8562(8)		8563(2)	52
8702(17)	$(1/2^+, 3/2^+, 5/2^+)$	8746(3)	53
8789(6)	$3/2^+, 5/2^+$	8788(3)	54
8813(15)		8815(3)	55
8878(22)	$(1/2^+, 3/2^+, 5/2^+)$	8904(6)	56
8969(20)		8973(4)	57
9004(20)		9001(3)	58
9155.2(12)	$(13/2^+)$	9155.2*	59
		[9293(2)]	60
		[9415(5)]	61
		[9499(8)]	62
		[9561(10)]	63
9606(14)		[9612(4)]	64
		[9641(4)]	65
		[9777(2)]	66
9853(12)		9831(4)	67
10146.2(11)	$(13/2^-)$	10146.2*	68
		[10282(4)]	69
		[10360(4)]	70
10577(13)		[10610(5)]	71
		[10800(5)]	72

The 6377 keV level. References [7,27,29,34] have assigned the spin-parity of the 6377 keV state to be $9/2^-$. The present deuteron angular distribution data are best fit by an $\ell = 5$ angular-momentum transfer, which leads to assignments of $9/2^-$ and $11/2^-$ for this state [see Fig. 3(f)]. Owing to the previous experimental results [7,27,29,34], we adopt $J^\pi = 9/2^-$ for this state.

The 6390.8 keV level. This state was observed at five angles (see Figs. 1 and 2). On the focal plane at positions corresponding to where this state appears at $\theta_{\rm lab} = 10^\circ$, 20°, and 22°, a broad peak was observed, whose shape was best reproduced with a doublet consisting of this state and the 6377 keV state (see Fig. 4).

TABLE III. Optical model parameters for DWBA analysis. For $p + n$ interaction, see text.

Reaction Channel	V_0 (MeV)	W_D (MeV)	r_0 (fm)	a (fm)	r_0' (fm)	a' (fm)	r_{0c} (fm)	$\lambda_{\rm SO}$
$p + ^{32}$S	47.1	6.87	1.18	0.66	1.18	0.66	1.18	
$d + ^{31}$S	90	25	1.25	0.62	1.30	0.58	1.18	
$n + ^{31}$S	56	1.20	0.65					251[a]

[a]Thomas spin-orbit factor [24].

The number of excited states in ^{31}S in the vicinity of $E_x = 6.4$ MeV has been a matter of discussion [8,28]. The most recent mass-31 evaluation [49] considered three

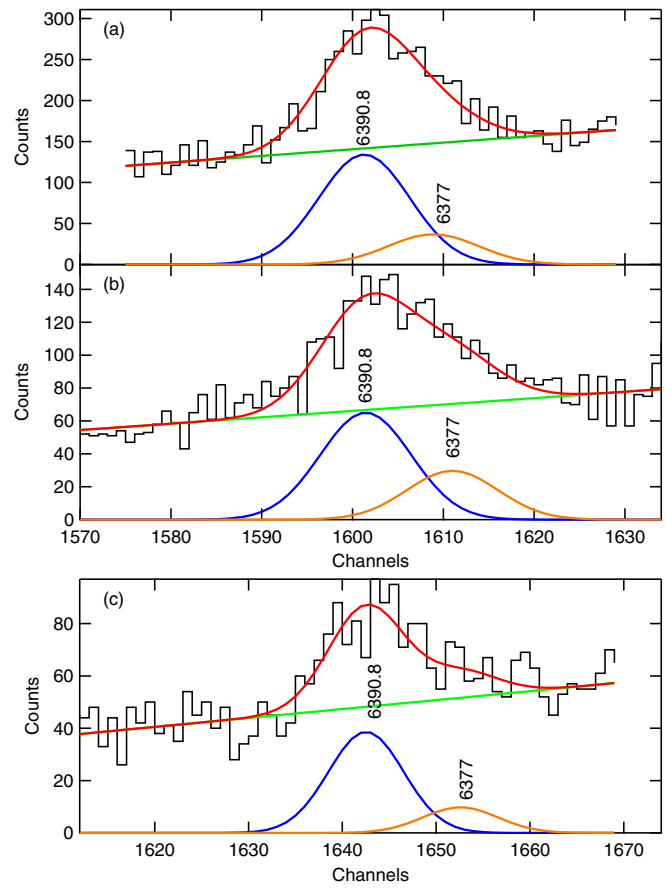

FIG. 4. Partial deuteron spectra from the ^{32}S(p, d) ^{31}S reaction, measured at (a) 22°, (b) 20°, and (c) 10°, which illustrate the individual Gaussian fits (in blue and orange), the total fits (in red), and the linear baselines (in green) for the states observed near $E_x = 6.4$ MeV labeled with energies (in keV). Peak fitting was performed by using the MINUIT package [57] for PYTHON [58]. The channel numbers are different due to kinematics shift. The spectra are aligned by eye for clarity. χ^2_ν of the fits varies between 1.36 at $\theta_{\rm lab} = 10^\circ$ to 1.58 at $\theta_{\rm lab} = 22^\circ$. All spectra are obtained using the CdS target. The 6377 keV state is respectively observed with a statistical significance of 1, 4.2, and 1.9 standard deviations at 10°, 20°, and 22° above the background expectations, respectively.

states in this region, namely, 6392.43(22) keV based on Refs. [27,29], 6394.36(22) keV based on Refs. [7,23,26–28,56], and 6401(3) keV based on Refs. [7,24,26,28]. More recently, another state was observed at 6390.2(7) keV [33,35] and most likely this state is not the same as the 6392.43 keV state because their spin-parity assignments are determined to be different. The J^π values for the 6390, 6392, and 6394 keV states have been assigned to be $3/2^+$ [33,35], $5/2^+$ [27,29,34], and $11/2^+$ [23,27,29], respectively. The spin-parity of the 6401 keV state is still experimentally unconstrained. It is tentatively estimated to be $7/2^-$ based on mirror state assignments performed in Ref. [28], and such assignments for the ^{31}S–^{31}P analog states are challenging and still quite uncertain. Our experimental resolution is not sufficient to resolve these states. Our observed state at $E_x = 6390.8(17)$ keV is in agreement within 1σ with both $E_x = 6392.43(22)$ keV reported in Refs. [27,29] and $E_x = 6390.2(7)$ keV reported in Refs. [33,35]. It is also consistent within 2σ with the $E_x = 6394.2(2)$ keV from Refs. [27,29]. What we have observed in our spectra may actually be a convolution of the 6390, 6392, and 6394 keV states. In that case, one would expect to see that the angular distribution data does not match with the individual J^π values ($3/2^+$, $5/2^+$, and $11/2^+$, respectively) but rather with the sum of the three. However, our angular distribution data are fit best with $J^\pi = 3/2^+$ and $J^\pi = 5/2^+$ [see Fig. 3(g)]. So it seems that the 6394 keV state may not be present in our spectra, which could be the case if it is not preferentially populated by a single-neutron removal process, e.g., via the (p, d) reaction. Our result seems to indicate that the (p, d) reaction tends to preferentially populate the $3/2^+$ and/or $5/2^+$ states near 6390 keV.

The 6542 keV level. At $\theta_{\rm lab} = 10^\circ$ and $\theta_{\rm lab} = 20^\circ$ in the present work, this state is weakly populated as a doublet with another state at 6585(2) keV. The latter level vanishes at $\theta_{\rm lab} = 22^\circ$ and $\theta_{\rm lab} = 45^\circ$, leaving the 6542 keV state as a singlet which is most prominently populated at $\theta_{\rm lab} = 45^\circ$ (see Fig. 2). Reference [27] reported that the contribution of this state to the ^{30}P$(p, \gamma)^{31}$S rate is significant. However, two measurements [7,27,29] have derived inconsistent J^π values for it. This source of ambiguity in the data available in the literature should be addressed because it reduces the confidence in the determination of the corresponding resonance strength, required for the rate calculation, as pointed out in Ref. [8]. The spin-parity of the 6542 keV level has been tentatively assigned to be $(7/2, 9/2)$ in Ref. [7]. But Refs. [27,29] assigned a firm $J^\pi = 3/2^-$. More recently, Ref. [34] assumed the J^π value of this state as $7/2^+$ (based on a recent re-analysis of light-ion transfer data [32]) and its contribution to the rate was modest. The present deuteron angular distribution data fit well with $\ell = 4,\ 5,\ 6$ transfers. Therefore, we tentatively assign $J^\pi = (7/2^+,\ 9/2^-,\ 11/2^+)$ to this state, which is consistent with the assignments made in Refs. [7,34] if we adopt $J^\pi = 7/2^+$. The $J^\pi = 3/2^-$ can be clearly ruled out from our data [see Fig. 3(h)], making the contribution of this state to the ^{30}P$(p, \gamma)^{31}$S reaction rate less significant since this state cannot be populated with an $\ell = 1$ angular-momentum transfer. We would like to also point out that the present angular distribution of this state and that of the 5402 keV state appear to be rather featureless. Compound nuclear reaction mechanisms may have a contribution to the populations of these weak excited states giving the total angular distribution profile shown by the data and resulting in total differential cross sections that are relatively flat for these two states. However, we consider this contribution to be small at 34.5 MeV/u beam energy, and therefore have not accounted for it. According to Ref. [59], the contribution from the direct reaction begins to dominate at energies above 10 MeV. Therefore, since the direct reaction contribution is most likely dominant in our case, it is unlikely that any *residual* compound contribution would make up for the difference between the 62° data point and the $3/2^-$ DWBA curve for the 6542 keV state. Likewise for the $5/2^+$ assignment for the 5402 keV state.

The 6636 keV level. This state is populated weakly at four angles in the present work (see Figs. 1 and 2). Its spin-parity is tentatively established to be $9/2^-$ in Ref. [49] based on the measurements of Refs. [7,23,27–29]. The present deuteron angular distribution data are reasonably fit with $J^\pi = 7/2^+$, $9/2^\pm$, and $11/2^+$ [see Fig. 3(i)]. Since the spin-parity assignment for this state is already tentatively established in the literature, we adopt $J^\pi = 9/2^-$.

The 6720 and 6749 keV levels. At all angles except 45°, where this region is obscured by ^{11}C, we observe a peak (labeled as peak 28/29 in Figs. 1 and 2) whose energy is consistent with (i) the 6720 keV state [49] at 27.5° and 62°, and (ii) the 6749 keV state [49] at 10°, 20°, and 22°. The FWHM of the peak we observe (peak 28/29) is comparable to that of a single state but from the energies we obtain, it seems to be an unresolved doublet. Therefore, we are unable to provide independent energy measurements for these two states from our data.

The 6833.9 keV level. The spin-parity of this level was first assigned to be $11/2^-$ in Ref. [23], which was excluded from the tentative assignments of $1/2^+$ to $9/2^-$ given to this state in Ref. [26]. Parikh *et al.* later confirmed $J = 11/2$ for this state in their ^{31}P$(^3$He$, t)^{31}$S measurement [7]. The present deuteron angular distribution data agrees best with $J^\pi = 9/2^-,\ 11/2^-$; however, the fit obtained with $J^\pi = 7/2^+$ assignment is also reasonable [see Fig. 3(j)].

The 7035.4 keV level. We observe a prominent peak at all angles except at $\theta_{\rm lab} = 27.5^\circ$. Its spin-parity is tentatively established to be $(1/2, 3/2, 5/2)^+$ from previous work [24,56,60,61]. The present deuteron angular distribution data do not agree with $J^\pi = 1/2^+$ but the fits obtained with $J^\pi = 3/2^+$ and $J^\pi = 5/2^+$ are in good agreement with the data [see Fig. 3(k)].

The 7157.7 keV level. This is a state observed at all six angles measured in our experiment. It has been observed in various previous experiments [23,24,26,35,56,61]. Reference [26] provides tentative spin assignments of $3/2$ and $5/2$ with a firm positive parity and Ref. [35] determines the J^π value to be $5/2^+$. This is in excellent agreement with our deuteron angular distribution plot for this state [see Fig. 3(l)], so we adopt the latter assignment.

V. CONCLUSIONS

Precise knowledge of energies and spin-parity assignments of resonances above the proton threshold [$S_p =$

6130.9(4) keV [19]] in ^{31}S is required for an accurate determination of the ^{30}P$(p, \gamma)^{31}$S reaction rate at the temperature range of $0.1 \leqslant T \leqslant 1.5$ GK, corresponding to explosive hydrogen burning in classical novae and type-I x-ray bursts. Understanding this rate, in turn, leads to a more complete picture of the origin of SiC presolar grains, which show excesses in ^{30}Si; an improved constraint of nova models; an advance in understanding nova thermometers; a tighter constraint on the abundance ratio of Si/H, which acts as a nova mixing meter; and progress in accurately determining the nucleosynthesis and energy generation of type-I x-ray bursts.

We have investigated the nuclear structure of ^{31}S via the ^{32}S$(p, d)^{31}$S reaction with a superior ($\geqslant$ a factor of two) energy resolution, when averaged over angles, with respect to that of the previous (p, d) measurement [24], and have observed 19 proton-bound states and 53 proton resonances in ^{31}S. With a few exceptions, our derived excitation energies are in good agreement within one standard deviation with those obtained in the previous work.

In particular, we have observed a state at 6390.8(17) keV. Our measured energy is consistent within 1σ with $E_x =$ 6390.2(7) keV measured in a previous β-delayed γ-decay study [33,35], as well as with $E_x = 6392.43(22)$ keV measured previously using Gammasphere [27,29]. These two measurements determine different spin-parity assignments to these states but the present angular distribution (and therefore our J^π assignment) is consistent with both.

Spin-parity assignments were performed in the present work for several ^{31}S states. This work specifically resolves the discrepancy in the spin and parity of the 6542 keV state, showing that it is not $J^\pi = 3/2^-$ as determined in Ref. [29]. As a consequence, the contribution of this state to the ^{30}P$(p, \gamma)^{31}$S reaction rate is likely downgraded, consistent with what is shown in Ref. [34]. In addition, our work helps solidify the spin and parity assignments for the 6377 and 6636 keV states.

The most recent evaluation of the ^{30}P$(p, \gamma)^{31}$S reaction rate was carried out in Ref. [34], where it was shown that the rate is significantly smaller than the shell-model rate calculated in Ref. [62] at low temperatures (0.1–0.17 GK). At higher temperatures, the rate was dominated by the $E_x =$ 6390.2(7) keV, $J^\pi = 3/2^+$ state, whose resonance strength is currently relying on the theoretical calculations. Given that the present ^{31}S excitation energies and J^π assignments are consistent with those of Ref. [34], we did not recalculate the ^{30}P$(p, \gamma)^{31}$S reaction rate.

Future work should focus on more progress in the determination of the spin-parities of the 6160, 6357, and 6583 keV states (energies are taken from Ref. [49]) to try to confirm the tentative assignments of Ref. [34]. Furthermore, the spin-parity of the 6401 keV state is still experimentally unconstrained. Consequently, Ref. [34] calculated the most recent ^{30}P$(p, \gamma)^{31}$S reaction rate excluding this state due to the uncertainties involved with estimating its resonance strength. Moreover, the proton widths and resonance strengths of many of the astrophysically important ^{31}S states are based on theoretical predictions. We would also like to note that a $1/2^-$ excited state has been predicted [30,62,63] to exist within the astrophysical range of interest for novae in ^{31}S. However, this state has not been observed so far. Future experiments should shed light on these issues.

ACKNOWLEDGMENTS

We would like to thank B. Singh for his assistance with the data analysis, the WNSL staff for their contributions, and S. Kubono for his valuable comments. This work was supported by the Natural Sciences and Engineering Research Council of Canada; the US Department of Energy under Grants No. DE-FG02-91ER40609, No. DE-AC02-06CH11357, No. DE-FG02-97ER41020, and No. DE-SC0016052; the US National Science Foundation under Grants No. PHY-1102511, No. PHY-1565546, and No. PHY-1913554; and the Japan Society for the Promotion of Science Core-to-Core Program on International Research Network for Exotic Femto Systems under Grant No. 18002.

[1] J. José and C. Iliadis, Rep. Prog. Phys. **74**, 096901 (2011).
[2] C. Iliadis, A. E. Champagne, J. José, S. Starrfield, and P. Tupper, Astrophys. J. Suppl. Ser. **142**, 105 (2002).
[3] J. José, M. Hernanz, and C. Iliadis, Nucl. Phys. A **777**, 550 (2006).
[4] P. A. Denissenkov, J. W. Truran, M. Pignatari, R. Trappitsch, C. Ritter, F. Herwig, U. Battino, K. Setoodehnia, and B. Paxton, Mon. Not. R. Astron. Soc. **442**, 2058 (2014).
[5] S. Starrfield, C. Iliadis, and W. R. Hix, Publ. Astron. Soc. Pac. **128**, 051001 (2016).
[6] J. José, *Stellar Explosions: Hydrodynamics and Nucleosynthesis* (CRC Press, Taylor and Francis, Boca Raton, 2016).
[7] A. Parikh, K. Wimmer, T. Faestermann, R. Hertenberger, J. José, R. Longland, H.-F. Wirth, V. Bildstein, S. Bishop, A. A. Chen *et al.*, Phys. Rev. C **83**, 045806 (2011).
[8] C. Wrede, AIP Adv. **4**, 041004 (2014).
[9] S. Amari, X. Gao, L. R. Nittler, E. Zinner, J. José, M. Hernanz, and R. S. Lewis, Astrophys. J. **551**, 1065 (2001).
[10] L. N. Downen, C. Iliadis, J. José, and S. Starrfield, Astrophys. J. **762**, 105 (2013).
[11] K. J. Kelly, C. Iliadis, L. Downen, J. José, and A. Champagne, Astrophys. J. **777**, 130 (2013).
[12] S. E. Woosley and R. E. Taam, Nature (London) **263**, 101 (1976).
[13] H. Schatz and K. E. Rehm, Nucl. Phys. A **777**, 601 (2006).
[14] J. L. Fisker, H. Schatz, and F.-K. Thielemann, Astrophys. J. Suppl. Ser. **174**, 261 (2008).
[15] H. Schatz, A. Aprahamian, J. Görres, M. Wiescher, T. Rauscher, J. F. Rembges, F.-K. Thielemann, B. PfeIffer, P. Möller, K.-L. Kratz *et al.*, Phys. Rep. **294**, 167 (1998).
[16] A. Parikh, J. José, F. Moreno, and C. Iliadis, Astrophys. J., Suppl. Ser. **178**, 110 (2008).
[17] R. H. Cyburt, A. M. Amthor, R. Ferguson, Z. Meisel, K. Smith, S. Warren, A. Heger, R. D. Hoffman, T. Rauscher, A. Sakharuk *et al.*, Astrophys. J. Suppl. Ser. **189**, 240 (2010).

[18] J. José, F. Moreno, A. Parikh, and C. Iliadis, Astrophys. J. Suppl. Ser. **189**, 204 (2010).

[19] M. Wang, G. Audi, F. G. Kondev, W. J. Huang, S. Naimi, and X. Xu, Chin. Phys. C **41**, 030003 (2017).

[20] G. Audi, F. G. Kondev, M. Wang, B. Pfeiffer, X. Sun, J. Blachot, and M. MacCormick, Chin. Phys. C **36**, 1157 (2012).

[21] D. A. Hutcheon *et al.*, TRIUMF EEC proposal S1108, https://dragon.triumf.ca/experiments/S1108_200607S.pdf (unpublished).

[22] D. G. Jenkins, C. J. Lister, M. P. Carpenter, P. Chowdhury, N. J. Hammond, R. V. F. Janssens, T. L. Khoo, T. Lauritsen, D. Seweryniak, T. Davinson *et al.*, Phys. Rev. C **72**, 031303(R) (2005).

[23] D. G. Jenkins, A. Meadowcroft, C. J. Lister, M. P. Carpenter, P. Chowdhury, N. J. Hammond, R. V. F. Janssens, T. L. Khoo, T. Lauritsen, D. Seweryniak *et al.*, Phys. Rev. C **73**, 065802 (2006).

[24] Z. Ma, D. W. Bardayan, J. C. Blackmon, R. P. Fitzgerald, M. W. Guidry, W. R. Hix, K. L. Jones, R. L. Kozub, R. J. Livesay, M. S. Smith *et al.*, Phys. Rev. C **76**, 015803 (2007).

[25] C. Wrede, J. A. Caggiano, J. A. Clark, C. M. Deibel, A. Parikh, and P. D. Parker, Phys. Rev. C **76**, 052802(R) (2007).

[26] C. Wrede, J. A. Caggiano, J. A. Clark, C. M. Deibel, A. Parikh, and P. D. Parker, Phys. Rev. C **79**, 045803 (2009).

[27] D. T. Doherty, G. Lotay, P. J. Woods, D. Seweryniak, M. P. Carpenter, C. J. Chiara, H. M. David, R. V. F. Janssens, L. Trache, and S. Zhu, Phys. Rev. Lett. **108**, 262502 (2012).

[28] D. Irvine, A. A. Chen, A. Parikh, K. Setoodehnia, T. Faestermann, R. Hertenberger, H.-F. Wirth, V. Bildstein, S. Bishop, J. A. Clark *et al.*, Phys. Rev. C **88**, 055803 (2013).

[29] D. T. Doherty, P. J. Woods, G. Lotay, D. Seweryniak, M. P. Carpenter, C. J. Chiara, H. M. David, R. V. F. Janssens, L. Trache, and S. Zhu, Phys. Rev. C **89**, 045804 (2014).

[30] M. Bouhelal and F. Haas, Eur. Phys. J. Plus **131**, 226 (2016).

[31] A. Saastamoinen, A. Kankainen, and L. Trache, Eur. Phys. J. Plus **131**, 272 (2016).

[32] A. Parikh, C. Wrede, and C. Fry, Eur. Phys. J. Plus **131**, 345 (2016).

[33] M. B. Bennett, C. Wrede, B. A. Brown, S. N. Liddick, D. Pérez-Loureiro, D. W. Bardayan, A. A. Chen, K. A. Chipps, C. Fry, B. E. Glassman *et al.*, Phys. Rev. Lett. **116**, 102502 (2016).

[34] A. Kankainen, P. J. Woods, H. Schatz, T. Poxon-Pearson, D. T. Doherty, V. Bader, T. Baugher, D. Bazin, B. A. Brown, J. Browne *et al.*, Phys. Lett. B **769**, 549 (2017).

[35] M. B. Bennett, C. Wrede, S. N. Liddick, D. Pérez-Loureiro, D. W. Bardayan, B. A. Brown, A. A. Chen, K. A. Chipps, C. Fry, B. E. Glassman *et al.*, Phys. Rev. C **97**, 065803 (2018).

[36] K. Setoodehnia, A. A. Chen, J. Chen, J. A. Clark, C. M. Deibel, S. D. Geraedts, D. Kahl, P. D. Parker, D. Seiler, and C. Wrede, Phys. Rev. C **82**, 022801(R) (2010).

[37] K. Setoodehnia, Ph.D. thesis, McMaster University, 2011 (unpublished); http://digitalcommons.mcmaster.ca/opendissertations/6313/.

[38] K. Setoodehnia, A. A. Chen, D. Kahl, T. Komatsubara, J. José, R. Longland, Y. Abe, D. N. Binh, J. Chen, S. Cherubini *et al.*, Phys. Rev. C **87**, 065801 (2013).

[39] S. Burcher, Ph.D. thesis, The University of Tennessee, Knoxville 2019 (unpublished); https://trace.utk.edu/islandora/object/utk.ir.td:12720/datastream/PDF/download/citation.pdf.

[40] C. Fry, Ph.D. thesis, Michigan State University, 2018 (unpublished); https://d.lib.msu.edu/etd/19526/datastream/OBJ/View/

[41] http://www.srim.org/; See also http://srim.org/SRIM/SRIMPICS/STOPPLOTS.htm.

[42] W. N. Lennard, K. Setoodehnia, A. A. Chen, and J. Hendriks, Nucl. Instrum. Methods Phys. Res., Sect. B **269**, 2726 (2011).

[43] C. Wrede, K. Deryckx, B. M. Freeman, A. García, G. C. Harper, A. S. C. Palmer, D. A. Short, and D. I. Will, Nucl. Instrum. Methods Phys. Res., Sect. B **268**, 3482 (2010).

[44] J. H. Kelley, E. Kwan, J. E. Purcell, C. G. Sheu, and H. R. Weller, Nucl. Phys. A **880**, 88 (2012).

[45] F. Ajzenberg-Selove, Nucl. Phys. A **523**, 1 (1991).

[46] M. S. Basunia, Nucl. Data Sheets **112**, 1875 (2011).

[47] G. Lotay, P. J. Woods, D. Seweryniak, M. P. Carpenter, H. M. David, R. V. F. Janssens, and S. Zhu, Phys. Rev. C **84**, 035802 (2011).

[48] A. Parikh, K. Wimmer, T. Faestermann, R. Hertenberger, H.-F. Wirth, A. A. Chen, J. A. Clark, C. M. Deibel, C. Herlitzius, R. Krücken *et al.*, Phys. Rev. C **84**, 065808 (2011).

[49] B. S. C. Oullette, Nucl. Data Sheets **114**, 209 (2013).

[50] M. Wang, G. Audi, A. H. Wapstra, F. G. Kondev, M. MacCormick, X. Xu, and B. Pfeiffer, Chin. Phys. C **36**, 1603 (2012).

[51] A. Kankainen, T. Eronen, D. Gorelov, J. Hakala, A. Jokinen, V. S. Kolhinen, M. Reponen, J. Rissanen, A. Saastamoinen, V. Sonnenschein *et al.*, Phys. Rev. C **82**, 052501(R) (2010).

[52] C. Iliadis, *Nuclear Physics of Stars*, 1st ed. (Wiley-VCH, Weinheim, 2007).

[53] P. D. Kunz, DWUCK5, http://spot.colorado.edu/~kunz/DWBA.html.

[54] R. L. Kozub, Phys. Rev. **172**, 1078 (1968).

[55] J. R. V. Reid, Ann. Phys. (NY) **50**, 411 (1968).

[56] J. Vernotte, G. Berrier-Ronsin, S. Fortier, E. Hourani, A. Khendriche, J. M. Maison, L.-H. Rosier, G. Rotbard, E. Caurier, and F. Nowacki, Nucl. Phys. A **655**, 415 (1999).

[57] F. James and M. Roos, Comput. Phys. Commun. **10**, 343 (1975).

[58] https://pypi.org/project/iminuit/.

[59] G. R. Satchler, *Introduction to Nuclear Reactions*, 2nd ed. (MacMillan Education Ltd., Hampshire, England, 1990), p. 68.

[60] P. M. Endt, Nucl. Phys. A **633**, 1 (1998).

[61] A. Kankainen, T. Eronen, S. P. Fox, H. O. U. Fynbo, U. Hager, J. Hakala, J. Huikari, D. G. Jenkins, A. Jokinen, S. Kopecky *et al.*, Eur. Phys. J. A **27**, 67 (2006).

[62] B. A. Brown, W. A. Richter, and C. Wrede, Phys. Rev. C **92**, 069901(E) (2015).

[63] B. A. Brown, W. A. Richter, and C. Wrede, Phys. Rev. C **89**, 062801(R) (2014).